THE JOURNAL OF PHYSICAL CHEMISTRY LETTERS
A JOURNAL OF THE AMERICAN CHEMICAL SOCIETY

pubs.acs.org/JPCL

Letter

Coordination Changes in Densified Aluminate Glass upon Compression up to 65 GPa: A View from Solid-State Nuclear Magnetic Resonance

Shujia Li, Jin Jung Kweon, Seoyoung Lee, A Chim Lee, and Sung Keun Lee*

Cite This: *J. Phys. Chem. Lett.* 2023, 14, 2078−2086

Read Online

ACCESS | Metrics & More | Article Recommendations | Supporting Information

ABSTRACT: Deciphering the structural evolution in irreversibly densified oxide glasses is crucial for fabricating functional glasses with tunable properties and elucidating the nature of pressure-induced anomalous plastic deformation in glasses. High-resolution NMR spectroscopy quantifies atomic-level structural information on densified glasses; however, its application is limited to the low-pressure range due to technical challenges. Here, we report the first high-resolution NMR spectra of oxide glass compressed by diamond anvil cells at room temperature, extending the pressure record of such studies from 24 to 65 GPa. The results constrain the densification path through coordination transformation of Al cations. Based on a statistical thermodynamic model, the stepwise changes in the Al fractions of oxide glasses and the effects of network polymerization on the densification paths are quantified. These results extend the knowledge on densification of the previously unattainable pressure conditions and contribute to understanding the origin of mechanical strengthening of the glasses.

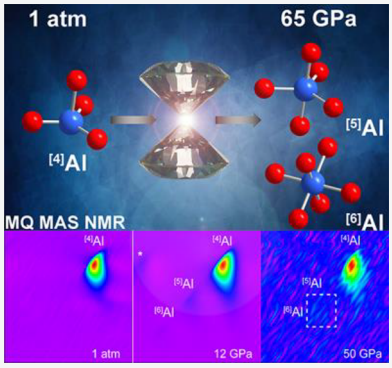

Oxide glasses undergo irreversible deformation upon extreme compression, permanently modifying the density and related properties after pressure release.[1−3] Deciphering the nature of pronounced irreversible densification is a long-standing interest in materials science since densified glasses tend to show improved hardness and fracture toughness.[4−9] The detailed nature of the permanent densification of oxide glass is crucial for understanding deformation mechanisms under sharp contact loading, as well as manufacturing glasses with tunable physical characteristics.[10] Oxide glasses are among the major constituents of the basaltic oceanic crust that form deep in Earth's mid-ocean ridges and are subject to densification during subduction, while they may form crystalline materials in contact with aqueous fluids.[11,12] Crystalline and noncrystalline aluminum-rich oxides in chondrites under shock compression and recovery record key information on high-pressure (HP) impact events in the early solar system.[13,14] Clarifying the structural transitions in oxide glass during irreversible densification is, therefore, vital for rebuilding the geological processes in planetary surfaces and interiors.

The structural origins of permanent densification in glasses at ambient temperature (cold compression)[15] and high temperature (hot compression)[16] include changes in the short-range structure, such as the cation coordination environments,[15,17−19] medium-range structure, particularly beyond the second coordination environment,[20−23] and topology of the network[4,24] (see Supporting Information S1 for detailed information regarding the factors that influence the degree of densification). Among these structural responses, short-range scale reconstruction controls the mechanical properties of glasses.[8] Despite its importance, the experimental detection of densified glass structures is a fundamental challenge owing to their intrinsic disorder and weak response to common experimental probes. Solid-state nuclear magnetic resonance (NMR) directly quantifies the coordination environment of constituent cations, the connectivity among those cations, and the topological disorder.[25−27] Progress has been made in high-resolution NMR research of densified oxide glasses, revealing the cation coordination environments in oxide glasses quenched from melts up to 16 GPa,[17,18,28−32] and preferential coordination transformation in distinct framework cations (e.g., Si and B) above 6 GPa.[19] These results constrain the pressure-induced changes in transport properties and configurational entropy of compressed glasses. A recent study of structural transitions in cold-compressed aluminosilicate glass up to 24 GPa revealed three pressure ranges with distinct degrees of coordination transformation,[15] which represents the highest pressure of such studies for oxide glasses (see refs 33 and 34 and references therein). Note that all of these

Received: January 18, 2023
Accepted: February 15, 2023
Published: February 17, 2023

https://doi.org/10.1021/acs.jpclett.3c00174
J. Phys. Chem. Lett. 2023, 14, 2078−2086

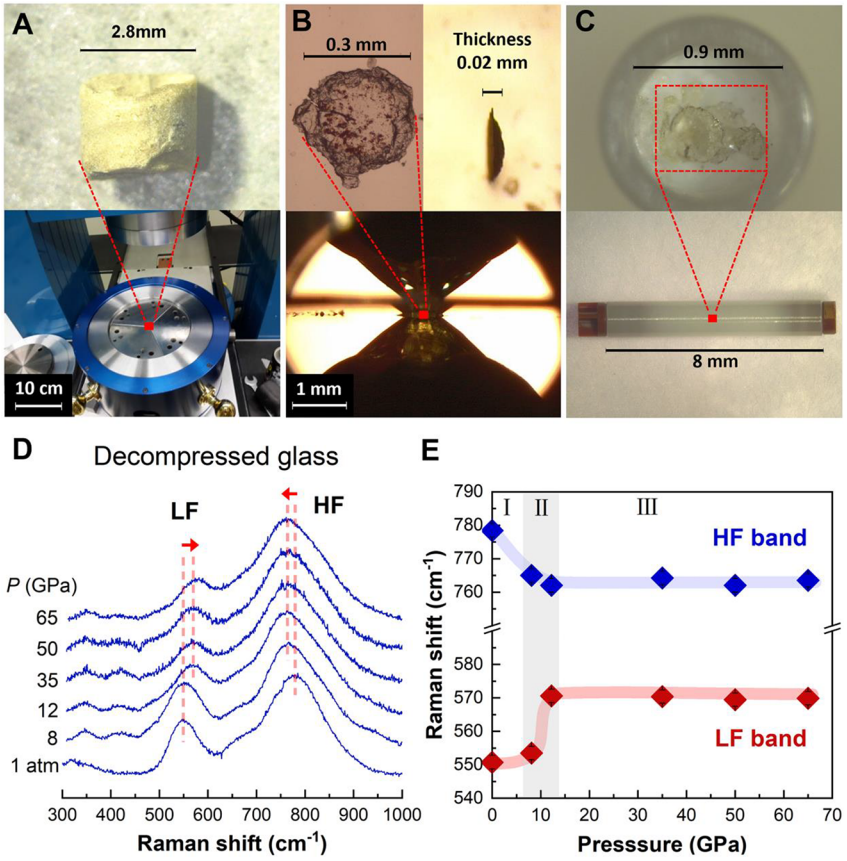

Figure 1. Optical photos of densified C13A7 glass and equipment used in ^{27}Al 3QMAS NMR experiments. (A) Glass decompressed from 12 GPa and the multianvil press. (B) Glass decompressed from 50 GPa and the diamond anvil cell. (C) 50 GPa-decompressed glass and rotor used in ^{27}Al 3QMAS NMR experiments for glasses quenched from 35 to 65 GPa. (D) Raman spectra of C13A7 glass decompressed from various peak pressures, as labeled. The spectra were collected at ambient pressure. (E) Evolution of Raman band positions with increasing peak pressures. The data points represent the frequencies where Raman bands have the maximum intensity. The gray shaded area indicates the pressure range in which the Raman bands drastically change. The lines are guides for the eye.

compressed glasses used in NMR studies have been synthesized by a large-volume multianvil press (LVP).

To further delve into the details of the current understanding of permanent densification, it is necessary to study the configuration changes under compression at higher pressures. Diamond anvil cells (DACs) can be a feasible approach that generates much higher-pressure conditions (e.g., refs 35 and 36 and references therein). However, they have not been utilized in high-resolution solid-state NMR studies. This is because the DAC-compressed sample volume (~0.007 mm^3) is ~4−6 orders of magnitude smaller than that of the LVP-compressed sample (~12 mm^3). Probing high-resolution NMR signals during the spinning of such limited samples has not yet been achieved. In the present study, we achieved a technological breakthrough by collecting the high-resolution NMR spectra of DAC-compressed materials. The pressure condition of the high-resolution NMR study was significantly extended to 65 GPa (from earlier high-pressure record of 24 GPa[15]). The current results provide the first insight into permanent densification under lower mantle pressures.

Calcium aluminate ($CaO-Al_2O_3$) glasses have technological applications in material physics[37] as they show sapphirelike infrared transparency,[38] have a bulk modulus of 123 GPa (1.45 times that of S-glass, which has the highest modulus of commercial glass fibers),[39] and have potential for amorphous laser emitting materials.[40] Ca-aluminate glasses are the parent compounds of a rare room-temperature electride and a glassy superconductor.[41−43] Furthermore, alumina glass films deform plastically without brittle fracture under indentation (and thus densification) at room temperature.[44] Previous pioneering studies of $CaAl_2O_4$ glass by high-pressure X-ray scattering,[45,46] Raman spectroscopy,[47] the decompressed glasses up to 16 GPa using NMR[17] indeed provided key insights, but the structural origins of peculiar properties remain to be revealed. Particularly, detailed structural origins of the irreversible densification paths for Ca-aluminate glasses under pressure greater than 16 GPa have been anticipated. Here, irreversible Al coordination changes in $13CaO{\cdot}7Al_2O_3$ (C13A7) glass are characterized by ^{27}Al NMR upon extreme compression to 65 GPa, providing the first direct evidence of Al coordination changes upon lower mantle pressure (at ~1500 km depth of the Earth) and insights into the origins of mechanical strengthening of the prototypical glass formers. Based on a statistical thermodynamic model,[15] we quantified the topological evolution of Ca-aluminate glass up to 65 GPa and discussed the effect of network polymerization on the nature of the irreversible densification paths.

Figure 1A−C shows the experimental procedures and protocols used in the current study (see Supporting Information S2 for a detailed description of materials and methods). The C13A7 glass was loaded into a multianvil apparatus and compressed at 8 and 12 GPa (Figure 1A). The

https://doi.org/10.1021/acs.jpclett.3c00174
J. Phys. Chem. Lett. 2023, 14, 2078−2086

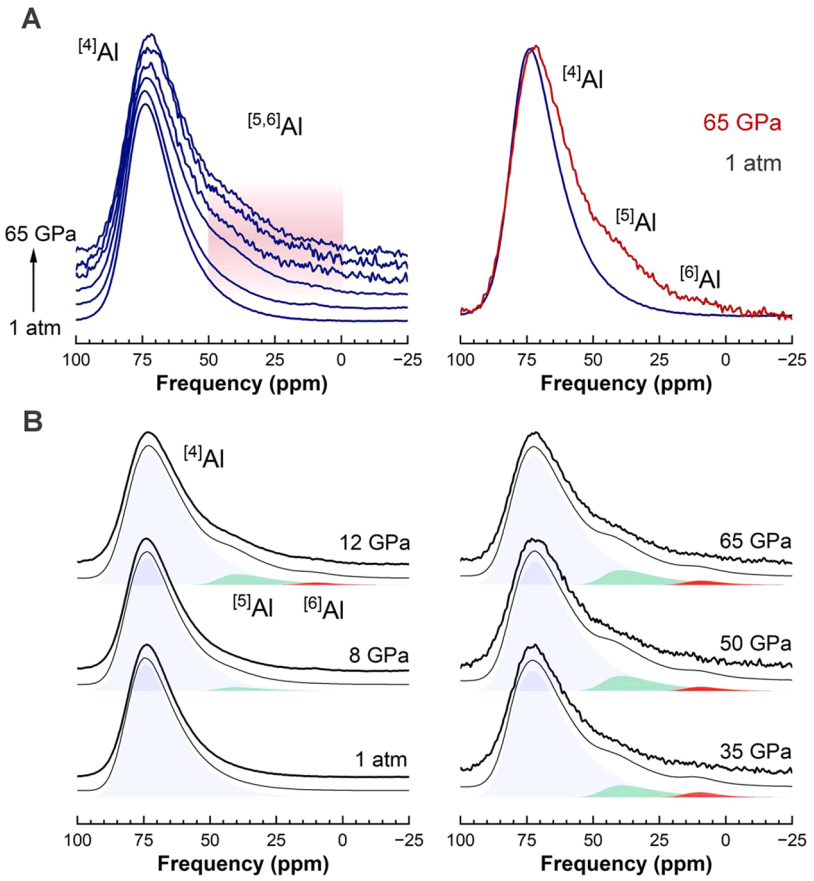

Figure 2. (A) 1D ^{27}Al MAS NMR spectra for irreversibly densified C13A7 glasses with various peak pressures as labeled. (B) ^{27}Al MAS NMR spectra with simulation results for decompressed glasses up to 65 GPa. The NMR spectra for the empty rotor and Teflon inset used in the ^{27}Al NMR measurements are shown in Figure S5. Considering negligible ^{27}Al signals from the rotors and stators, all the spectral intensities are contributed solely by the C13A7 glasses.

densified C13A7 glasses recovered from 35, 50, and 65 GPa were pressed by DACs with 300 and 400 μm culet diamonds at room temperature (Figure 1B). Because of the size limitation of the sample chamber in the DAC, the synthesis process was repeated 15−20 times at each pressure to obtain enough densified glasses for NMR measurements. The total weight of the DAC-compressed glasses was less than 0.02 mg. The densified glasses were packed into a 1.3 mm diameter rotor for NMR measurements (Figure 1C). To collect NMR signals from such a small sample mass, additional effort was made to optimize the measurement parameters, and an extended collection time was adopted to reduce the signal-to-noise ratio. Two-dimensional (2D) NMR spectra under magic-angle spinning (MAS) at 50 GPa were collected for 48 days.

The in situ Raman spectra of the C13A7 glass up to 50 GPa and the pressure-induced shift of spectral patterns up to 13 GPa are shown in Figures S1 and S2 (data processing details can be found in Supporting Information S3). The Raman spectra for C13A7 glass at ambient pressure and those up to 8 GPa show two main bands: a high-frequency (HF) band in the region of 700−850 cm^{-1} and a low-frequency (LF) band at ∼500−600 cm^{-1}. The HF and the LF band were attributed to Al−O stretching vibrations and to the delocalized vibrations of the intertetrahedral Al−O−Al linkage, respectively.[47−50] In previous Raman studies of Ca-aluminate glasses, the bands centered at ∼730, 780, and 780−910 cm^{-1} stem from $^{[4]}$Al−O stretching vibrations of the Q^2, Q^3, and Q^4 groups (Q^n describes the AlO units coordinated by n number of bridging oxygens.)[48] Therefore, the pressure-induced increase in the 855 cm^{-1} band is attributed to a decrease in Q^2 and Q^3 groups and the increasing number of Q^4 group. From 8 to 13 GPa, the LF (and HF) bands shifted to higher (and lower) frequencies; the pressure-induced LF band shift indicates a decreasing Al−O−Al angle and/or an increasing fraction of smaller rings.[47] The HF band shift toward a lower frequency suggests a gradual pressure-induced increase in the average Al−O bond length.[47] Above 12 GPa, the band intensities decreased dramatically and became negligible, after which (>15 GPa) a broad band at ∼750 cm^{-1} dominated. These changes are due to the presence of highly coordinated Al,[47] while confirming the proportions of $^{[5,6]}$Al species is necessary (see below). With a further increase in pressure, the change in Raman patterns is quite ambiguous, mostly due to pressure-induced weakening and broadening of the Raman characteristics of glasses and the interference of the diamond window.[51]

Figure 1D,E shows the Raman spectra and position of the LF/HF bands of glasses decompressed to ambient pressure from various peak pressures (i.e., the highest pressure where decompression started), revealing the topological evolution of the glassy network during decompression and irreversible densification. When decompressed from 8 GPa, the HF band shifted to a lower frequency. When decompressed from pressures ≥12 GPa, the LF band intensity decreased. The HF and LF bands shifted to lower and higher frequencies, respectively, which reflects changes in the Al−O bond length

https://doi.org/10.1021/acs.jpclett.3c00174
J. Phys. Chem. Lett. 2023, 14, 2078−2086

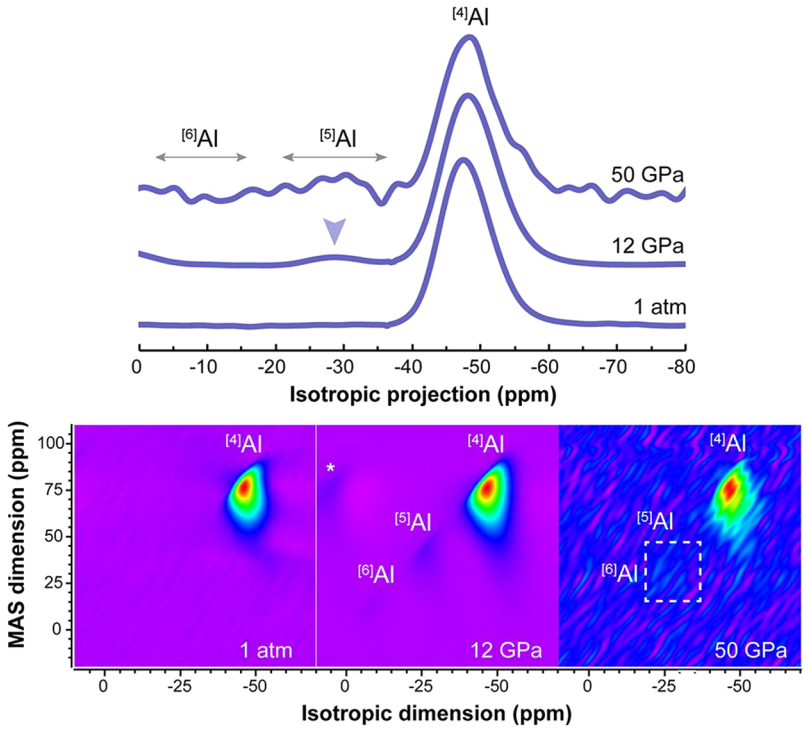

Figure 3. Total isotropic projection (top) and full 2D ^{27}Al 3QMAS NMR spectra (bottom) for decompressed C13A7 glasses after cold compression up to 50 GPa. The area in the dashed square corresponds to the $^{[5]}$Al species.

or the Al−O−Al angle upon permanent densification. The change in the spectra mainly occurred in the pressure range 8−12 GPa. As the peak pressure increased, the left shoulder of the HF band (~700−750 cm^{-1}) diminished while the right side of the HF band (~850 cm^{-1}) was enhanced, indicating the increase in Al Q^4 species and thus the degree of polymerization. It should also be noted that the overall profile of ex situ Raman spectra of glasses decompresses from P > 12 GPa are different from the in situ Raman spectra under the corresponding pressures, but rather similar to that at lower pressures. This observation confirms that the pressure-induced structural change at peak pressure is overly relaxed back to that at lower pressure conditions. Despite the utility, the Raman results do not provide information regarding the explicit Al coordination numbers in the densified glasses, particularly above 12−15 GPa.

The structural transitions in the irreversibly densified C13A7 glass were captured in the ^{27}Al NMR results. Figure 2A shows the ^{27}Al MAS NMR spectra of the C13A7 glass at ambient pressure and glass *decompressed* from various pressures up to 65 GPa. At 1 atm, a predominant 73 ppm peak was observed, corresponding to $^{[4]}$Al. As the peak pressure increased above 8 GPa, a spectral intensity at 39 ppm developed, which corresponds to $^{[5]}$Al. When the peak pressure increased above 12 GPa, a small feature with a maximum at 9 ppm was also observed corresponding to $^{[6]}$Al (see refs 17, 28, and 52 and references therein). Peaks due to $^{[4,5,6]}$Al's are unambiguously observed in the NMR spectra of the aluminate glasses decompressed from 35, 50, and 65 GPa. The $^{[5,6]}$Al peak intensities increased with increasing pressure up to 35 GPa, but above 35 GPa, the increase in $^{[5,6]}$Al peaks was negligible (despite the uncertainty in measurements). A comparison of the spectra at ambient pressure and 65 GPa (Figure 2A, right) clearly shows the formation of $^{[5,6]}$Al peaks, providing explicit evidence for the structural evolutions involving the coordination environment in the densified C13A7 glasses. The observed presence of $^{[5,6]}$Al species quenched to ambient pressure can serve as a useful structural proxy of the permanent deformation of densified aluminate glass.

To obtain quantitative fractions of the $^{[4,5,6]}$Al sites in C13A7 glasses, the one-dimensional (1D) ^{27}Al MAS NMR results were fitted using the *CzSimple* function for $^{[4,5,6]}$Al sites in DmFit software.[53] Figure 2B shows the simulated results (see below for the fractions of $^{[n]}$Al versus pressures); when decompressed from 8 GPa, ~2.7% of $^{[5]}$Al was observed. From ambient pressure to 8 GPa, the $^{[5]}$Al fraction increased at an average pressure dependence of ~0.3%/GPa. With further compression to 12 GPa, the fraction of $^{[5,6]}$Al dramatically increased to 8.0%, with approximately 1.3%/GPa. Above 12 GPa, the increasing rate of the fractions of $^{[5,6]}$Al slowed and reached a plateau. When decompressed from 35 GPa, the fraction of $^{[5,6]}$Al increased to 10.0%. When decompressed from 50 and 65 GPa, the $^{[5,6]}$Al fractions were ~11−12%. The average pressure dependence of the $^{[5,6]}$Al fractions in the large pressure range of 12−65 GPa was quite low (0.06%/GPa). Therefore, the observed coordination transformations of Al in the compressed C13A7 glass showed three distinct pressure ranges. First, when decompressed from lower pressures (below 8 GPa), the structural changes were rather minor. The detection limit of Al coordination environments in the current study is approximately 0.3%. Therefore, a minor fraction of $^{[5,6]}$Al (below the detection limit) may be present at lower pressure conditions. In the transition pressure region (i.e., from ~8 to 12 GPa in the current study), the atomic arrangement underwent a steep change, whereas pressure-induced coordination changes were relatively minor when decompressed from pressures above 12 to 65 GPa.

https://doi.org/10.1021/acs.jpclett.3c00174
J. Phys. Chem. Lett. 2023, 14, 2078−2086

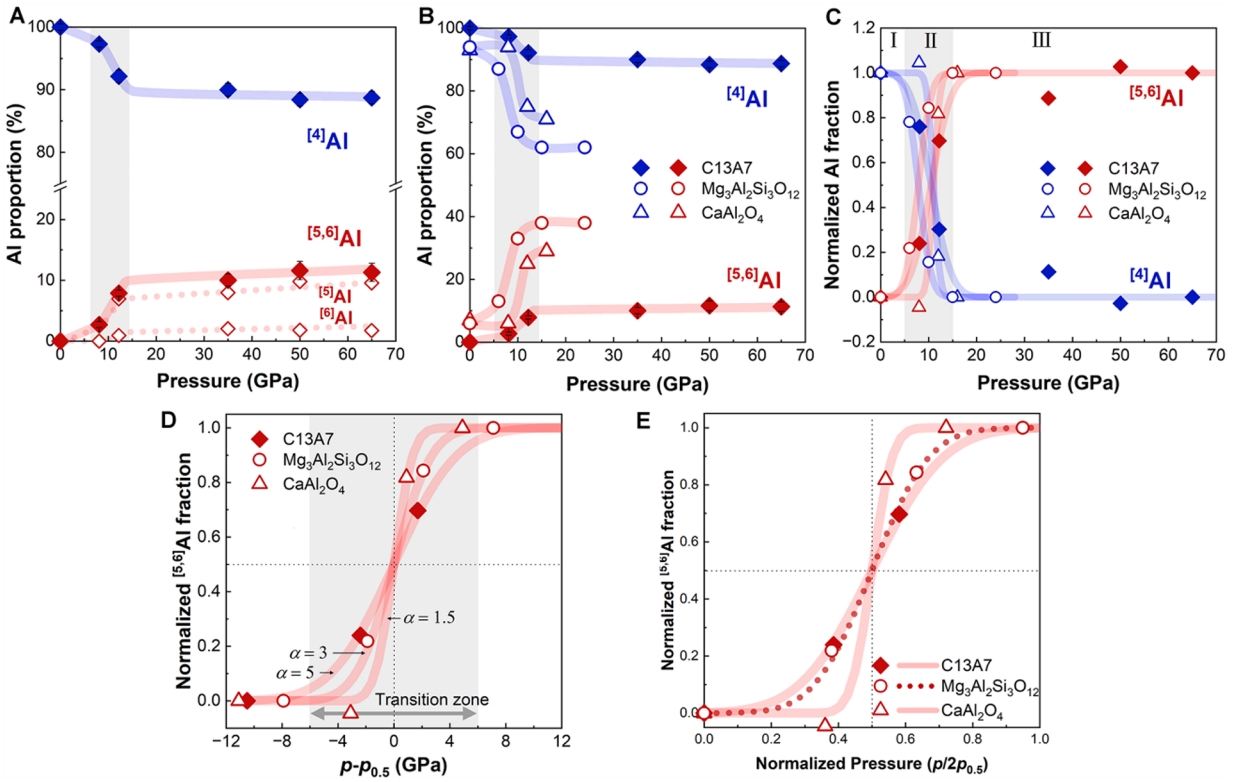

Figure 4. (A) Variation of the proportions of four- (blue ◆), five-, and six-coordinated Al (red ◇) ($^{[5,6]}$Al, red ◆) of decompressed C13A7 glasses after cold compression up to 65 GPa. The gray shaded area indicates the pressure range of drastic coordination environmental changes. The lines are guides for the eye. (B) Comparison of the $^{[4]}$Al and $^{[5,6]}$Al fraction of C13A7 (current study), $CaAl_2O_4$[17], and $Mg_3Al_2Si_3O_{12}$[15] glasses. The lines are guides for the eye. (C) Variation of normalized $^{[4,5,6]}$Al fraction, $\overline{X^{[n]}Al(p)}$, with varying peak pressures (i.e., $[X^{[n]}Al(p) - X^{[n]}Al_{24GPa}]/[X^{[n]}Al_{1atm} - X^{[n]}Al_{24GPa}]$). The red lines are simulated results using eq 1. The blue lines are calculated by $\overline{X^{[4]}Al(p)} = 1 - \overline{X^{[5,6]}Al(p)}$. Normalized fractions of $^{[5,6]}$Al $[\overline{X^{[5,6]}Al(p)}]$ with (D) the $p' = p - p_{0.5}$ and (E) the normalized pressure ($\overline{p} = p/2p_{0.5}$). The lines are simulated results using eq 1. The error bars in panels A and B only represent the uncertainties of *CzSimple* simulations. The uncertainties of NMR measurements caused by the small sample mass are unknown.

Figure 3 shows the total isotropic projections of the 2D ^{27}Al triple quantum (3Q) MAS NMR results and full 2D spectra for decompressed C13A7 glasses under pressure. While $^{[4]}$Al is predominant at 1 atm, the spectrum at 12 GPa reveals three well-resolved peaks due to 4,5,6-coordinated Al species. As the sample volume decreases, the intensity of the whole spectrum and the signal-to-noise ratio declined at 50 GPa. Nevertheless, the results revealed the presence of $^{[5]}$Al in the C13A7 glass. The current spectra highlight that high-resolution 2D 3QMAS NMR can be realized for the compressed ~0.01 mg sample.

The evolution of the NMR parameters used in the simulations of ^{27}Al 1D MAS spectra can be found in Table S1 and Figure S6. The ^{27}Al quadrupolar coupling constant (C_q) measures the extent of deviation from perfect cubic symmetry.[54] The C_q of $^{[4]}$Al increased from 6.9 MHz (1 atm) to 7.8 MHz (65 GPa). The C_q of $^{[5]}$Al increased from 6.8 MHz (8 GPa) to 7.7 MHz (65 GPa). The intense increase of $^{[4]}$Al C_q and $^{[5]}$Al C_q occurred in the pressure range 8−12 GPa, which is the identical pressure range in which the Al coordination number increased sharply. These changes indicate that the network distortion and the topological disorder around Al increased prominently at elevated peak pressure along the transition region. As network polymerization often increases by annihilating nonbridging oxygen (NBO),[15,18,26] the following mechanism for the aluminate glass is established: Ca-NBO (Ca−O−$^{[4]}$Al) + $^{[4]}$Al−O−$^{[4]}$Al ⇒ $^{[4]}$Al−O−$^{[5]}$Al−O−$^{[4]}$Al···Ca*, where Ca* refers to a charge-balancing cation.

The current ^{27}Al NMR results for compressed C13A7 glass can be compared with those of other oxide glasses irreversibly densified under lower pressure conditions. Figure 4A,B shows the pressure-induced changes in the $^{[n]}$Al fraction of the C13A7 glass in the current study and of the permanently densified $CaAl_2O_4$[17] (up to 16 GPa) and $Mg_3Al_2Si_3O_{12}$[15] (up to 24 GPa) in previous ^{27}Al NMR studies. The current study more than doubled the pressure record of high-pressure NMR studies (from 24 to 65 GPa). The molar ratio of the network modifier and framework Al atoms [R = (MgO+CaO)/Al_2O_3] is used as an index to describe the polymerization degree of aluminate glass networks; a smaller R represents a more polymerized network up to 1, where the network is fully polymerized.[55] The presence of modifiers with large cationic potential (c/r, where c and r are the charge and ionic radius of cations), e.g., Mg^{2+}, increases the fraction of $^{[5]}$Al at 1 atm.[54] Compared with the current C13A7 glass (R = 1.86), $CaAl_2O_4$ with R of 1 and $Mg_3Al_2Si_3O_{12}$ glass (R = 3) with Mg^{2+} as a network modifier showed a larger $^{[5]}$Al fraction at 1 atm. After decompression from high pressures, the $^{[5,6]}$Al fractions in these glasses were higher than those of the C13A7 glass. This confirms that the polymerization degree and the $^{[5,6]}$Al fractions in the glasses at ambient pressure affect the overall configurational changes of the decompressed glasses, as explored by the earlier pioneering studies.[28]

https://doi.org/10.1021/acs.jpclett.3c00174
J. Phys. Chem. Lett. 2023, 14, 2078−2086

Whereas the fractions of $^{[4,5,6]}$Al are all different for these glasses, the formation paths of $^{[5,6]}$Al in all three glasses show similar patterns, with a sharp increase in the $^{[5,6]}$Al population in the pressure range ~6−12 GPa (i.e., transition zone), and then reaching a saturation value above ~12−15 GPa, above which the fractions are unchanged.[15] The current study, together with those results at lower pressure conditions,[15,17] confirms a universal densification pathway for permanent structural changes in glass networks. To model such evolution paths, we explored the pressure-driven increase in normalized $^{[n]}$Al coordination number.[15] In Figure 4C, the fractional changes of $^{[4,5,6]}$Al in C13A7, $CaAl_2O_4$,[17] and $Mg_3Al_2Si_3O_{12}$[15] glass were normalized to the fractions at the highest pressures in the corresponding studies [$\overline{X^{[4,5,6]}Al(p)}$]; thus, consistent trends in the fractions of various glasses are clearly shown. The differences between the various glasses are mainly in the central pressure and width of the transition zone. The three-step changing paths of the normalized fraction, $\overline{X^{[5,6]}Al(p)}$, of various glasses are described by the following model:[15]

$$\overline{X^{[5,6]}Al(p)} = 1 - \frac{1}{2} \times \mathrm{erfc}\left(\frac{p - p_{0.5}}{\alpha}\right) \quad (1)$$

where $p_{0.5}$ represents the central pressure where the $\overline{X^{[n]}Al(p)}$ reaches half of its maximum; and α is a dimensionless constant corresponding to the width of the transition zone, which reflects the extent of rigidity of the Al network in the pressure-induced coordination transition. The red lines in Figure 4C show the best simulations of the normalized fractions using eq 1 (see Supporting Information S5). In earlier studies, the observed trend in the $^{[5,6]}$Al fractions was positively correlated with variations of the residual density of glasses,[15] suggesting a correspondence between the short-range structures and macroscopic densification of oxide glasses. Because we do not have the bulk density data for the current glasses, further confirmation between Al coordination number in the decompressed glass and bulk density may not be fully established. Nevertheless, the identical patterns for normalized Al coordination numbers indicate that a similar correlation might be driven for the Ca−Al glass. Further experimental data with bulk density information may confirm the postulate.

By analyzing the variation of α and $p_{0.5}$ in different glasses (Table 1), the factors affecting the permanent densification path can be determined. In Figure 4D, the true pressure, p, is adjusted to $p' = p - p_{0.5}$ to effectively highlight the difference in α values of different glasses. The depolymerized C13A7 (R = 1.86) and $Mg_3Al_2Si_3O_{12}$ glasses (R = 3) correspond to remarkably larger α (wider transition zones) than the more polymerized $CaAl_2O_4$ (R = 1) and $CaAl_2Si_2O_8$ glasses (R = 1) (the latter from ab initio simulations[56]); based on this trend, it can be concluded that more depolymerized networks are more susceptible to coordination transformation upon compression and decompression. It is currently unclear whether the presence of a modifier with large cationic potential, such as Mg^{2+} (c/r of ~2.8), affects α, as more experimental data are necessary. Nevertheless, the presence of Mg^{2+} also led to a smaller $p_{0.5}$ [compared to Ca^{2+} (c/r of ~2.0)] and induced structural modification (i.e., Al coordination change) at lower pressure conditions (see Table 1). This can be attributed to the additional degree of disorder induced by Mg^{2+}.[54] Figure 4E shows the evolution of the normalized fractions with normalized pressure ($p/2p_{0.5}$). All $^{[5,6]}$Al fractions of glasses can be described using eq 1, confirming the universal irreversible densification path for oxide glasses, in which the clear effect of the concentration of non-network formers on network densification is also highlighted.

The $^{[5,6]}$Al fractions in the decompressed glasses were well-correlated with the residual glass density.[15] Furthermore, the bulk modulus of anorthite glass under low pressure (<10 GPa) and that under high pressure (>10 GPa) are largely different, consistent with the changes in Al coordination in the glasses.[56] These findings suggests that the fractions of $^{[5,6]}$Al in these glasses can be useful to infer the elastic properties of the glasses. While further experimental and modeling efforts are certainly necessary to confirm the nature of irreversible structural transitions in decompressed oxide glasses, the current results up to the unprecedented pressure condition of 65 GPa suggest that disequilibrium densification accompanied by extreme compression may render a greater degree of instability in oxide glass networks, compared with those compressed at lower pressure conditions as also addressed in earlier studies of glasses and amorphization of high-pressure polymorphs during compression and/or decompression.[57,58] We expect that decompressed aluminate glass may experience a second steep increase to another plateau in the Al coordination environment, which may occur when the glass undergoes cold compression to extreme conditions, forming $^{[>6]}$Al species or network domains with larger fractions of $^{[5,6]}$Al. As glass undergoing compression at an elevated temperatures exhibits a greater degree of densification than glass undergoing cold compression (at room temperature),[16] the second plateau may be achieved by compressing glass under higher temperatures. We note that the focus of the current study is to show pressure-induced structural changes in coordination number (i.e., short-range structures). Those associated beyond second coordination shells (i.e., medium-range structures) may also contribute to the overall changes in density as demonstrated in earlier studies of glass densification at high temperatures.[59]

We report the first high-resolution NMR spectra for aluminate glass that underwent permanent densification up to 65 GPa. This unambiguous experimental evidence constrains the densification path of Al cations and confirms the contribution of short-range structural changes to permanent densification. The coordination environment of Al changed remarkably in a narrow transition zone from 8 to 12 GPa, characterized by a sharply increasing $^{[5,6]}$Al fraction. In

Table 1. Fitting Parameters ($p_{0.5}$ and α) for the $^{[5,6]}$Al Fraction and the Molar Ratio of Non-Network Former and Al Ions R [(CaO+MgO)/Al_2O_3] for Diverse Aluminate Glasses[a]

composition	$p_{0.5}$ (GPa)	α	R	ref
$13CaO{\cdot}7Al_2O_3$	10.5	5 ± 1	1.86	current study
$Mg_3Al_2Si_3O_{12}$	7.9	3	3	Lee et al. (2020)[15]
$CaAl_2O_4$	11.1	1.5	1	Amin et al. (2012)[17]
$CaAl_2Si_2O_8$[b]	9 (10.3)	2 (2.1)	1	Ghosh et al. (2018)[56]

[a]The Al coordination was gained from the NMR studies ($13CaO{\cdot}7Al_2O_3$, $Mg_3Al_2Si_3O_{12}$, and $CaAl_2O_4$) and first-principles molecular dynamics simulations ($CaAl_2Si_2O_8$) of glasses undergoing cold compression. [b]As the fraction data near the transition zone being deficient, the simulated parameters $p_{0.5}$ and α for the $^{[5,6]}$Al fraction of $CaAl_2Si_2O_8$ glass have uncertainties larger than those of the other glasses. For reference, the fitted $p_{0.5}'$ and α' for the residual densities of $CaAl_2Si_2O_8$ glass are provided in parentheses.

https://doi.org/10.1021/acs.jpclett.3c00174
J. Phys. Chem. Lett. 2023, 14, 2078−2086

contrast, the Al coordination environment did not change over a wide range from ∼35 to 65 GPa. This indicates that lower-pressure densification up to ∼12 GPa is sufficient to deform glass plastically. This may increase the yield strength of densified oxide glass, inducing mechanical hardening. More extensive studies with varying compositions and pressures are required to test the aforementioned hypothesis and the applicability of glasses under extreme conditions. Subsequent exploration may be able to achieve a tunable activation pressure for the large-degree densification of glass. The degree of rigidity of the Al network under pressure can be effectively modulated by changing the ratio of the framework and modifier and the type of modifier, which provides significant insights for tuning the processing technology and expanding the application scenarios of glass materials. In terms of geoscience, aluminum and calcium oxide are also among the most abundant components in the partial melts formed in the Earth's lower mantle.[60,61] The dramatic change of Al configuration in the upper mantle region may contribute to mechanical hardening and extend the elastic limit of the subducted noncrystalline oxides and silicates within basaltic crusts, while these glasses may be hydrated to form crystalline silicates. We expect that our ongoing studies of compressed glasses with varying compositions and temperatures under much extended pressure conditions may reveal additional mechanisms for permanent densification, such as second stage changes in Al and/or Si coordination numbers.

■ ASSOCIATED CONTENT

Supporting Information

The Supporting Information is available free of charge at https://pubs.acs.org/doi/10.1021/acs.jpclett.3c00174.

Previous studies of the irreversibly densified oxide glasses; material synthesis and experimental methods; processing method of high-pressure Raman spectra (in situ); in situ structural changes of $13CaO{\cdot}7Al_2O_3$ glass; modeling analysis of Al coordination change; structure of glass in $CaO-Al_2O_3$ join at ambient pressure; previous XRD studies; uncertainty of Al fractions; fractions, δ_{iso}, C_q, and FWHM of Al species; high-pressure Raman results; change of Raman band positions with increasing pressures; Raman vibrational peak of diamond; Raman spectra of C13A7 glass with background; ^{27}Al NMR spectra of empty rotor and rotor with Teflon inset; and quadrupolar coupling constant (C_q) (PDF)

■ AUTHOR INFORMATION

Corresponding Author

Sung Keun Lee − *Laboratory of Physics and Chemistry of Earth Materials, School of Earth and Environmental Sciences and College of Natural Sciences, Institute of Applied Physics, Seoul National University, Seoul 08826, South Korea;* orcid.org/0000-0002-3149-3421; Email: sungklee@snu.ac.kr

Authors

Shujia Li − *Laboratory of Physics and Chemistry of Earth Materials, School of Earth and Environmental Sciences, Seoul National University, Seoul 08826, South Korea*

Jin Jung Kweon − *Laboratory of Physics and Chemistry of Earth Materials, School of Earth and Environmental Sciences, Seoul National University, Seoul 08826, South Korea;* orcid.org/0000-0003-1961-3424

Seoyoung Lee − *Laboratory of Physics and Chemistry of Earth Materials, School of Earth and Environmental Sciences, Seoul National University, Seoul 08826, South Korea;* orcid.org/0000-0001-6572-9714

A Chim Lee − *Laboratory of Physics and Chemistry of Earth Materials, School of Earth and Environmental Sciences, Seoul National University, Seoul 08826, South Korea;* orcid.org/0000-0002-8279-2085

Complete contact information is available at: https://pubs.acs.org/10.1021/acs.jpclett.3c00174

Notes

The authors declare no competing financial interest.

■ ACKNOWLEDGMENTS

This work was supported by the Research Leader program of the National Research Foundation of Korea grants (No. NRF-2020R1A3B2079815) to S.K.L. We thank two anonymous reviewers for their constructive suggestions which greatly improved the quality of the manuscript.

■ REFERENCES

(1) Rouxel, T.; Ji, H.; Hammouda, T.; Moréac, A. Poisson's Ratio and the Densification of Glass under High Pressure. *Phys. Rev. Lett.* **2008**, *100* (22), 225501.

(2) Januchta, K.; Smedskjaer, M. M. Indentation Deformation in Oxide Glasses: Quantification, Structural Changes, and Relation to Cracking. *J. Non-Cryst. Solids: X* **2019**, *1*, 100007.

(3) Huang, L.; Kieffer, J. Amorphous-Amorphous Transitions in Silica Glass. I. Reversible Transitions and Thermomechanical Anomalies. *Phys. Rev. B* **2004**, *69* (22), 224203.

(4) Ji, H.; Keryvin, V.; Rouxel, T.; Hammouda, T. Densification of Window Glass under Very High Pressure and Its Relevance to Vickers Indentation. *Scr. Mater.* **2006**, *55* (12), 1159−1162.

(5) Kapoor, S.; Guo, X.; Youngman, R. E.; Hogue, C. L.; Mauro, J. C.; Rzoska, S. J.; Bockowski, M.; Jensen, L. R.; Smedskjaer, M. M. Network Glasses under Pressure: Permanent Densification in Modifier-Free $Al_2O_3-B_2O_3-P_2O_5-SiO_2$ systems. *Phys. Rev. Appl.* **2017**, *7* (5), No. 054011.

(6) Molnár, G.; Ganster, P.; Tanguy, A. Effect of Composition and Pressure on the Shear Strength of Sodium Silicate Glasses: an Atomic Scale Simulation Study. *Phys. Rev. E* **2017**, *95* (4), No. 043001.

(7) Deschamps, T.; Margueritat, J.; Martinet, C.; Mermet, A.; Champagnon, B. Elastic Moduli of Permanently Densified Silica Glasses. *Sci. Rep.* **2014**, *4* (1), 7193.

(8) Wu, J.; Gross, T. M.; Huang, L.; Jaccani, S. P.; Youngman, R. E.; Rzoska, S. J.; Bockowski, M.; Bista, S.; Stebbins, J. F.; Smedskjaer, M. M. Composition and Pressure Effects on the Structure, Elastic Properties and Hardness of Aluminoborosilicate Glass. *J. Non-Cryst. Solids* **2020**, *530*, 119797.

(9) Richet, P. *Encyclopedia of Glass Science, Technology, History, and Culture*; John Wiley & Sons, 2021.

(10) Wondraczek, L.; Bouchbinder, E.; Ehrlicher, A.; Mauro, J. C.; Sajzew, R.; Smedskjaer, M. M. Advancing the Mechanical Performance of Glasses: Perspectives and Challenges. *Adv. Mater.* **2022**, *34* (14), 2109029.

(11) Plank, T.; Langmuir, C. H. The Chemical Composition of Subducting Sediment and Its Consequences for the Crust and Mantle. *Chem. Geol.* **1998**, *145* (3−4), 325−394.

(12) Workman, R. K.; Hart, S. R. Major and Trace Element Composition of the Depleted MORB Mantle (DMM). *Earth and Planet. Sci. Lett.* **2005**, *231* (1−2), 53−72.

(13) Grossman, L.; Beckett, J. R.; Fedkin, A. V.; Simon, S. B.; Ciesla, F. J. Redox Conditions in the Solar Nebula: Observational,

Experimental, and Theoretical Constraints. *Rev. Mineral. Geochem.* **2008**, *68* (1), 93−140.
(14) Nakamura, T. Formation and evolution of carbonaceous asteroid Ryugu: Direct evidence from returned samples. *Science* **2022**, eabn8671.
(15) Lee, S. K.; Mun, K. Y.; Kim, Y. H.; Lhee, J.; Okuchi, T.; Lin, J. F. Degree of Permanent Densification in Oxide Glasses upon Extreme Compression up to 24 GPa at Room Temperature. *J. Phys. Chem. Lett.* **2020**, *11* (8), 2917−2924.
(16) Sun, N.; Mao, Z.; Zhang, X.; Tkachev, S. N.; Lin, J.-F. Hot Dense Silica Glass with Ultrahigh Elastic Moduli. *Sci. Rep.* **2022**, *12* (1), 13946.
(17) Amin, S. A.; Leinenweber, K.; Benmore, C. J.; Weber, R.; Yarger, J. L. Characterizing Pressure-Induced Coordination Changes in $CaAl_2O_4$ Glass Using ^{27}Al NMR. *J. Phys. Chem. C* **2012**, *116* (3), 2068−2073.
(18) Lee, S. K. Simplicity in Melt Densification in Multicomponent Magmatic Reservoirs in Earth's Interior Revealed by Multinuclear Magnetic Resonance. *Proc. Natl. Acad. Sci. U. S. A.* **2011**, *108* (17), 6847−6852.
(19) Lee, A. C.; Kim, E. J.; Lee, S. K. Pressure-Induced Structural Evolution in Boron-Bearing Model Rhyolitic Glasses under Compression: Implications for Boron Isotope Compositions and Properties of Deep Melts in Earth's Interior. *Geochim. Cosmochim. Acta* **2022**, *332*, 220−238.
(20) Lee, S. K.; Lee, A. C.; Kweon, J. J. Probing Medium-Range Order in Oxide Glasses at High Pressure. *J. Phys. Chem. Lett.* **2021**, *12* (4), 1330−1338.
(21) Neuville, D. R.; Le Losq, C. Link between Medium and Long-range Order and Macroscopic Properties of Silicate Glasses and Melts. *Rev. Mineral. Geochem.* **2022**, *87* (1), 105−162.
(22) Onodera, Y.; Kohara, S.; Salmon, P. S.; Hirata, A.; Nishiyama, N.; Kitani, S.; Zeidler, A.; Shiga, M.; Masuno, A.; Inoue, H.; Tahara, S.; Polidori, A.; Fischer, H. E.; Mori, T.; Kojima, S.; Kawaji, H.; Kolesnikov, A. I.; Stone, M. B.; Tucker, M. G.; McDonnell, M. T.; Hannon, A. C.; Hiraoka, Y.; Obayashi, I.; Nakamura, T.; Akola, J.; Fujii, Y.; Ohara, K.; Taniguchi, T.; Sakata, O. Structure and Properties of Densified Silica Glass: Characterizing the Order Within Disorder. *NPG Asia Mater.* **2020**, *12* (1), 85.
(23) Papadopoulos, A. G.; Tagiara, N. S.; Stavrou, E.; Li, F.; Yang, G.; Kamitsos, E. I. Pressure-Induced Structural Transformations and Electronic Transitions in TeO_2 Glass by Raman Spectroscopy. *J. Phys. Chem. Lett.* **2023**, *14* (2), 387−394.
(24) Trease, N. M.; Clark, T. M.; Grandinetti, P. J.; Stebbins, J. F.; Sen, S. Bond Length-Bond Angle Correlation in Densified Silica—Results from ^{17}O NMR Spectroscopy. *J. Chem. Phys.* **2017**, *146* (18), 184505.
(25) Stebbins, J. F.; Xue, X. NMR Spectroscopy of Inorganic Earth Materials. *Rev. Mineral. Geochem.* **2014**, *78* (1), 605−653.
(26) Lee, S. K.; Mosenfelder, J. L.; Park, S. Y.; Lee, A. C.; Asimow, P. D. Configurational Entropy of Basaltic Melts in Earth's Mantle. *Proc. Natl. Acad. Sci. U. S. A.* **2020**, *117* (36), 21938−21944.
(27) Lee, J.; Lee, W.; Kang, K.; Lee, T.; Lee, S. K. Layer-by-Layer Structural Identification of 2D Ruddlesden−Popper Hybrid Lead Iodide Perovskites by Solid-State NMR Spectroscopy. *Chem. Mater.* **2021**, *33* (1), 370−377.
(28) Yarger, J. L.; Smith, K. H.; Nieman, R. A.; Diefenbacher, J.; Wolf, G. H.; Poe, B. T.; McMillan, P. F. Al Coordination Changes in High-Pressure Aluminosilicate Liquids. *Science* **1995**, *270* (5244), 1964−1967.
(29) Allwardt, J. R.; Stebbins, J. F.; Terasaki, H.; Du, L.-S.; Frost, D. J.; Withers, A. C.; Hirschmann, M. M.; Suzuki, A.; Ohtani, E. Effect of Structural Transitions on Properties of High-Pressure Silicate Melts: ^{27}Al NMR, Glass Densities, and Melt Viscosities. *Am. Mineral.* **2007**, *92* (7), 1093−1104.
(30) Kanzaki, M.; Stebbins, J. F.; Xue, X. Characterization of Quenched High Pressure Phases in $CaSiO_3$ System by XRD and ^{29}Si NMR. *Geophys. Res. Lett.* **1991**, *18* (3), 463−466.
(31) Xue, X.; Stebbins, J. F.; Kanzaki, M.; McMillan, P. F.; Poe, B. Pressure-induced silicon coordination and tetrahedral structural changes in alkali oxide-silica melts up to 12 GPa: NMR, Raman, and infrared spectroscopy. *Am. Mineral.* **1991**, *76* (1−2), 8−26.
(32) Kim, E. J.; Kim, Y.-H.; Lee, S. K. Pressure-Induced Structural Transitions in Na−Li Silicate Glasses under Compression. *J. Phys. Chem. C* **2019**, *123* (43), 26608−26622.
(33) Lee, S. K. Effect of Pressure on Structure of Oxide Glasses at High Pressure: Insights from Solid-State NMR of Quadrupolar Nuclides. *Solid State Nucl. Magn. Reson.* **2010**, *38* (2−3), 45−57.
(34) Lee, S. K.; Parq, J.-H.; Yi, Y. S.; Lee, S.; Kim, H.-I.; Lee, S.-M.; Yu, J. Structure and Disorder in $MgSiO_3$ Glasses above Megabar Pressures via Nuclear Magnetic Resonance: DFT Calculations. *J. Am. Ceram. Soc.* **2022**, *105* (8), 5151−5166.
(35) Ji, C.; Li, B.; Liu, W.; Smith, J. S.; Majumdar, A.; Luo, W.; Ahuja, R.; Shu, J.; Wang, J.; Sinogeikin, S.; Meng, Y.; Prakapenka, V. B.; Greenberg, E.; Xu, R.; Huang, X.; Yang, W.; Shen, G.; Mao, W. L.; Mao, H.-K. Ultrahigh-Pressure Isostructural Electronic Transitions in Hydrogen. *Nature* **2019**, *573* (7775), 558−562.
(36) Kim, Y.-H.; Yi, Y. S.; Kim, H.-I.; Chow, P.; Xiao, Y.; Shen, G.; Lee, S. K. Pressure-Driven Changes in the Electronic Bonding Environment of GeO_2 Glass above Megabar Pressures. *J. Am. Chem. Soc.* **2022**, *144* (22), 10025−10033.
(37) Cormier, L. Glasses: Aluminosilicates. In *Encyclopedia of Materials: Technical Ceramics and Glasses*, 2021; pp 496−518.
(38) Sung, Y.; Kwon, S. Glass-Forming Ability and Stability of Calcium Aluminate Optical Glasses. *J. Mater. Sci. Lett.* **1999**, *18* (15), 1267−1269.
(39) Wallenberger, F.; Brown, S. High-Modulus Glass Fibers for New Transportation and Infrastructure Composites and New Infrared Uses. *Compos. Sci. Technol.* **1994**, *51* (2), 243−263.
(40) Denker, B. I.; Galagan, B. I.; Sverchkov, S. E. Laser Potential of Calcium Aluminate Glasses. *J. Non-Cryst. Solids* **2018**, *496*, 29−33.
(41) Kim, S. W.; Shimoyama, T.; Hosono, H. Solvated Electrons in High-Temperature Melts and Glasses of the Room-Temperature Stable Electride $[Ca_{24}Al_{28}O_{64}]^{4+}\cdot 4e^-$. *Science* **2011**, *333* (6038), 71−74.
(42) Kim, S. W.; Matsuishi, S.; Nomura, T.; Kubota, Y.; Takata, M.; Hayashi, K.; Kamiya, T.; Hirano, M.; Hosono, H. Metallic State in a Lime−Alumina Compound with Nanoporous Structure. *Nano Lett.* **2007**, *7* (5), 1138−1143.
(43) Miyakawa, M.; Kim, S. W.; Hirano, M.; Kohama, Y.; Kawaji, H.; Atake, T.; Ikegami, H.; Kono, K.; Hosono, H. Superconductivity in an Inorganic Electride $12CaO\cdot 7Al_2O_3$: e^-. *J. Am. Chem. Soc.* **2007**, *129* (23), 7270−7271.
(44) Frankberg, E. J.; Kalikka, J.; García Ferré, F.; Joly-Pottuz, L.; Salminen, T.; Hintikka, J.; Hokka, M.; Koneti, S.; Douillard, T.; Le Saint, B.; Kreiml, P.; Cordill, M. J.; Epicier, T.; Stauffer, D.; Vanazzi, M.; Roiban, L.; Akola, J.; Di Fonzo, F.; Levänen, E.; Masenelli-Varlot, K. Highly Ductile Amorphous Oxide at Room Temperature and High Strain Rate. *Science* **2019**, *366* (6467), 864−869.
(45) Drewitt, J. W.; Jahn, S.; Sanloup, C.; de Grouchy, C.; Garbarino, G.; Hennet, L. *Metter* Development of Chemical and Topological Structure in Aluminosilicate Liquids and Glasses at High Pressure. *J. Phys.: Condens. Metter* **2015**, *27* (10), 105103.
(46) Mei, Q.; Benmore, C. J.; Sampath, S.; Weber, J. K. R.; Leinenweber, K.; Amin, S.; Johnston, P.; Yarger, J. L. The Structure of Permanently Densified $CaAl_2O_4$ Glass. *J. Phys. Chem. Solids* **2006**, *67* (9−10), 2106−2110.
(47) Daniel, I.; McMillan, P. F.; Gillet, P.; Poe, B. T. Raman Spectroscopic Study of Structural Changes in Calcium Aluminate ($CaAl_2O_4$) Glass at High Pressure and High Temperature. *Chem. Geol.* **1996**, *128* (1−4), 5−15.
(48) McMillan, P.; Piriou, B. Raman Spectroscopy of Calcium Aluminate Glasses and Crystals. *J. Non-Cryst. Solids* **1983**, *55* (2), 221−242.
(49) McMillan, P.; Piriou, B.; Navrotsky, A. A Raman Apectroscopic Study of Glasses Along the Joins Silica-Calcium Aluminate, Silica-

https://doi.org/10.1021/acs.jpclett.3c00174
J. Phys. Chem. Lett. 2023, 14, 2078−2086

Sodium Aluminate, and Silica-Potassium Aluminate. *Geochim. Cosmochim. Acta* **1982**, *46* (11), 2021−2037.
(50) Mysen, B. O.; Virgo, D.; Kushiro, I. The Structural Role of Aluminum In Silicate Melts—a Raman Spectroscopic Study at 1 atm. *Am. Mineral.* **1981**, *66* (7−8), 678−701.
(51) Ardia, P.; Di Muro, A.; Giordano, D.; Massare, D.; Sanchez-Valle, C.; Schmidt, M. Densification Mechanisms of Haplogranite Glasses as a Function of Water Content and Pressure Based on Density and Raman Data. *Geochim. Cosmochim. Acta* **2014**, *138*, 158−180.
(52) Lee, S. K.; Lee, S. B.; Park, S. Y.; Yi, Y. S.; Ahn, C. W. Structure of Amorphous Aluminum Oxide. *Phys. Rev. Lett.* **2009**, *103* (9), No. 095501.
(53) Massiot, D.; Fayon, F.; Capron, M.; King, I.; Le Calvé, S.; Alonso, B.; Durand, J.-O.; Bujoli, B.; Gan, Z.; Hoatson, G. Modelling One- and Two-Dimensional Solid-State NMR Spectra. *Magn. Reson. Chem.* **2002**, *40* (1), 70−76.
(54) Park, S. Y.; Lee, S. K. Probing the Structure of Fe-Free Model Basaltic Glasses: A View from a Solid-State ^{27}Al and ^{17}O NMR Study of Na-Mg Silicate Glasses, Na_2O-MgO-Al_2O_3-SiO_2 Glasses, and Synthetic Fe-Free KLB-1 Basaltic Glasses. *Geochim. Cosmochim. Acta* **2018**, *238*, 563−579.
(55) Neuville, D. R.; Henderson, G. S.; Cormier, L.; Massiot, D. The structure of crystals, glasses, and melts along the CaO-Al_2O_3 join: Results from Raman, Al L- and K-edge X-ray absorption, and ^{27}Al NMR spectroscopy. *Am. Mineral.* **2010**, *95* (10), 1580−1589.
(56) Ghosh, D. B.; Karki, B. B. First-Principles Molecular Dynamics Simulations of Anorthite ($CaAl_2Si_2O_8$) Glass at High Pressure. *Phys. Chem. Miner.* **2018**, *45* (6), 575−587.
(57) Williams, Q.; Jeanloz, R. Spectroscopic Evidence for Pressure-Induced Coordination Changes in Silicate Glasses and Melts. *Science* **1988**, *239* (4842), 902−905.
(58) Mao, H. K.; Chen, L. C.; Hemley, R. J.; Jephcoat, A. P.; Wu, Y.; Bassett, W. A. Stability and Equation of State of $CaSiO_3$-Perovskite to 134 GPa. *Journal of Geophysical Research: Solid Earth* **1989**, *94* (B12), 17889−17894.
(59) Allwardt, J. R.; Stebbins, J. F.; Schmidt, B. C.; Frost, D. J.; Withers, A. C.; Hirschmann, M. M. Aluminum Coordination and the Densification of High-Pressure Aluminosilicate Glasses. *Am. Mineral.* **2005**, *90* (7), 1218−1222.
(60) Boehler, R.; Ross, M. Properties of Rocks and Minerals, High-Pressure Melting. In *Treatise on Geophysics*, 2nd ed.; Schubert, G., Ed.; Elsevier: Oxford, 2015; Chapter 2.22, pp 573−582.
(61) Pradhan, G. K.; Fiquet, G.; Siebert, J.; Auzende, A.-L.; Morard, G.; Antonangeli, D.; Garbarino, G. Melting of MORB at Core−Mantle Boundary. *Earth and Planet. Sci. Lett.* **2015**, *431*, 247−255.

https://doi.org/10.1021/acs.jpclett.3c00174
J. Phys. Chem. Lett. 2023, 14, 2078−2086